Tensions between direct measurements of the lens power spectrum from Planck data

Pavel Motloch[1] and Wayne Hu[2]

[1] *Kavli Institute for Cosmological Physics, Department of Physics, University of Chicago, Chicago, Illinois 60637, U.S.A*

[2] *Kavli Institute for Cosmological Physics, Department of Astronomy & Astrophysics, Enrico Fermi Institute, University of Chicago, Chicago, Illinois 60637, U.S.A*

We apply a recently developed method to directly measure the gravitational lensing power spectrum from CMB power spectra to the Planck satellite data. This method allows us to analyze the tension between the temperature power spectrum and lens reconstruction in a model independent way. Even when allowing for arbitrary variations in the lensing power spectrum, the tension remains at the 2.4σ level. By separating the lensing and unlensed high redshift information in the CMB power spectra, we also show that under ΛCDM the two are in tension at a similar level whereas the unlensed information is consistent with lensing reconstruction. These anomalies are driven by the smoother acoustic peaks relative to ΛCDM at $\ell \sim 1250 - 1500$. Both tensions relax slightly when polarization data are considered. This technique also isolates the one aspect of the lensing power spectrum that the Planck CMB power spectra currently constrain and can be straightforwardly generalized to future data when CMB power spectra constrain multiple aspects of lensing which are themselves correlated with lensing reconstruction.

I. INTRODUCTION

Measurements of anisotropies in the cosmic microwave background (CMB) have helped to establish ΛCDM as the standard cosmological model and measure its parameters with high precision. Currently, CMB data are precise enough to detect the effects of gravitational lensing (see [1] for a review) at high significance [2–11]. This secondary signal depends on growth of structure in the universe, which can be leveraged to measure better certain parameters in ΛCDM like the sum of the neutrino masses and search for new physics beyond it.

Information carried by the lensing potential ϕ can be recovered either by measuring its effect on CMB power spectra, in particular the smoothing of the acoustic peaks [12], or by higher point combinations of the temperature and polarization maps. The latter is possible, because gravitational lensing generates a correlation between measured CMB fields and their gradients [13]. This correlation can be used to reconstruct ϕ, for example using quadratic combinations of maps [14–16] or iterative approaches [17, 18]. The reconstructed potential then serves as a new observable whose power spectrum $C_L^{\phi\phi}$ contains cosmological information.

Within the context of ΛCDM, measurements of the Planck satellite show internal tension – at significance over 2σ – in the amount of lensing apparently present in the temperature power spectra data [19–22]. At the same time, the amount of lensing detected through the lensing reconstruction seems to be consistent with the ΛCDM model. Such tensions are interesting, as they could indicate residual systematics in the data, which would have to be understood before performing delensing using the reconstructed ϕ [23]. They might even represent hints of new physics beyond the ΛCDM model.

In this paper, we perform a model-independent investigation of $C_L^{\phi\phi}$ information in the Planck temperature and polarization power spectra and assess its tension with lensing reconstruction. As opposed to previous studies of the tension, which considered changes to only the amplitude of the gravitational lensing potential relative to the ΛCDM model, we allow for more general changes. This enables us to probe the possibility that models beyond ΛCDM might resolve this lensing tension.

Specifically, we implement the method introduced in [24, 25], in which the lensing potential is constrained directly. This method isolates the precise aspect of $C_L^{\phi\phi}$ that temperature and polarization power spectra constrain, which enables a more incisive and model-independent assessment of any tension with reconstruction. Additionally, this work represents the first test of the method on real data. This method will become increasingly useful in the future as CMB temperature and polarization power spectra constrain more than just the amplitude of the gravitational lensing potential and enable consistency tests that are largely immune to cosmic variance.

This paper is organized as follows. In §II we summarize the Planck likelihoods used in this work and introduce our technique for probing the gravitational lensing potential. In §III we use this method to derive Planck lensing constraints from CMB power spectra and lens reconstruction. In §IV we then evaluate the significance of the tensions between the two and with ΛCDM. We discuss our findings in §V.

II. LENSING METHODOLOGY

In this section we first introduce the data and analysis method used in this work. After that we detail the technique we use to directly measure the gravitational lensing potential from the data; this technique is employed to probe Planck lensing tensions in the later sections.

TABLE I. Planck likelihoods used in this work

Label	Power spectra	ℓ-range	Binned?	Name
`TT`	TT	$\ell \geq 30$	yes	`plik_dx11dr2_HM_v18_TT`
`TTTEEE`	TT,TE,EE	$\ell \geq 30$	yes	`plik_dx11dr2_HM_v18_TTTEEE`
`lowT`	TT	$\ell < 30$	no	`commander_rc2_v1.1_l2_29_B`
`lowTEB`	TT,TE,EE,BB	$\ell < 30$	no	`lowl_SMW_70_dx11d_2014_10_03_v5c_Ap`
`PP`	$\phi\phi$	$40 \leq \ell \leq 400$	yes	`smica_g30_ftl_full_pp`
`liteTT`	TT	$\ell \geq 30$	yes	`plik_lite_v18_TT`

A. Data sets and MCMC

For the analyses in this work we use the publicly released Planck 2015 likelihoods[*1] for the power spectra of the CMB temperature, polarization and of the gravitational lensing potential reconstructed from their maps as summarized in Table I. Joint use of multiple likelihoods will be denoted by a plus sign connecting them. For the analyses using only the lensing reconstruction likelihood `PP`, correction for the $N^{(0)}, N^{(1)}$ biases is performed using the best fit power spectra to `TT+lowTEB` likelihoods assuming the six parameter ΛCDM model. The likelihood `liteTT`, which we use for the lens principal component construction and checking robustness of the results below, is a high-ℓ temperature likelihood, with the foreground parameters pre-marginalized over. Otherwise, we marginalize over the standard foreground parameters with their default priors, where applicable.

For the analyses in this paper we use the Markov Chain Monte Carlo (MCMC) code CosmoMC[*2] [26] to sample the posterior probability in the various parameter spaces described in the next section. Each of our chains has a sufficient number of samples such that the Gelman-Rubin statistic $R-1$ [27] falls below 0.01.

B. Lens PC measurement technique

We can measure gravitational lensing of the CMB from both temperature and polarization power spectra and from lensing reconstruction. While lensing reconstruction maps directly measure the lens power spectrum $C_L^{\phi\phi}$, in the standard analysis of the temperature and polarization power lensing is inferred from the set of model parameters. This makes it difficult to compare these two distinct sources of lensing information directly since information from the latter is embedded in the cosmological parameter constraints. In this work we instead consider model-independent constraints on $C_L^{\phi\phi}$. For this purpose we introduce a basis of N effective parameters $\Theta^{(i)}$ which determine arbitrary variations around a fixed fiducial power spectrum $C_{L,\rm fid}^{\phi\phi}$ as

$$C_L^{\phi\phi} = C_{L,\rm fid}^{\phi\phi} \exp\left(\sum_{i=1}^{N} K_L^{(i)}\,\Theta^{(i)}\right). \qquad (1)$$

In this setup, constraining $\Theta^{(i)}$ from the data corresponds directly to constraining the gravitational lensing potential. This should be contrasted with the common approach of introducing a phenomenological parameter A_L which multiplies $C_L^{\phi\phi}$ at each point in the model space and cannot be so interpreted once model parameters are marginalized over.

We choose $K_L^{(i)}$ such that $\Theta^{(i)}$ correspond to N principal components (PCs) of the gravitational lensing potential best measured by the Planck lensed TT power spectrum. We determine them from the data covariance matrix provided with the Planck likelihood `liteTT` using a Fisher matrix construction; the resultant eigenmodes $K_L^{(i)}$ are shown in Fig. 1. The lowest variance mode peaks around $L = 100$ and is much better constrained than the second best constrained component; the Fisher matrix forecast predicts a factor of ~ 50 in the ratio of variances. This is largely because Planck data do not strongly constrain the BB power spectrum [28] or temperature multipoles above $\ell \approx 2000$, which are sensitive to smaller scale lenses. Because $K_L^{(i)}$ are smooth functions of L, we discretize $C_L^{\phi\phi}$ into bins of width $\Delta L = 5$ (see [24] for more details). Unless otherwise specified, we retain $N = 4$ PCs in order to fully characterize all sources of lensing information (see §III A).

In addition to these lens parameters we take the standard ΛCDM parameters for the unlensed CMB spectra: $\Omega_b h^2$, the physical baryon density; $\Omega_c h^2$, the physical cold dark matter density; n_s, the tilt of the scalar power spectrum; $\ln A_s$, its log amplitude at $k = 0.05$ Mpc^{-1}; τ the optical depth through reionization, and θ_*, the angular scale of the sound horizon at recombination. We use flat priors with uninformative ranges on these parameters.

In the MCMC analyses with $\Theta^{(i)}$, these cosmological parameters are still present and determine the "unlensed" CMB fluctuations at recombination as well as the background expansion. However, they do not affect the lens potential as they would in the standard analysis. We will refer to these parameters collectively as $\tilde{\theta}_A$, where the

[*1] https://www.cosmos.esa.int/web/planck/pla
[*2] https://github.com/cmbant/CosmoMC

TABLE II. ΛCDM parameters and their fiducial values for the lens PC construction[a].

Parameter	Fiducial value
$100\,\theta_*$	1.041
$\Omega_c h^2$	0.1197
$\Omega_b h^2$	0.02223
n_s	0.9658
$\ln(10^{10} A_s)$	3.049
τ	0.058

[a] In ΛCDM, these parameters also imply a Hubble constant of $h = 0.6733$.

tilde is to remind the reader that the gravitational lens potential is not changed by these parameters.

The fiducial cosmological model used to calculate $C^{\phi\phi}_{L,\rm fid}$ in Eq. (1) is taken from the best fit flat ΛCDM cosmological model, determined from `TT+lowTEB` likelihoods assuming no primordial tensor modes and minimal mass neutrinos ($\sum m_\nu = 60\,$meV). To reflect the latest results on the optical depth to recombination τ [29], we set τ to the value from that work and decrease A_s to keep $A_s e^{-2\tau}$ constant. A lower A_s tends to exacerbate the preference for anomalously high lensing in the temperature power spectrum within the ΛCDM context but here serves only as the baseline fiducial model against which to define $\Theta^{(i)}$. Values of the corresponding cosmological parameters are listed in Table II.

In models beyond ΛCDM, changes in the integrated Sachs-Wolfe (ISW) effect would typically affect data on the largest scales. In this work we are interested only in lensing-like effects and leave the ISW contribution at its ΛCDM value.

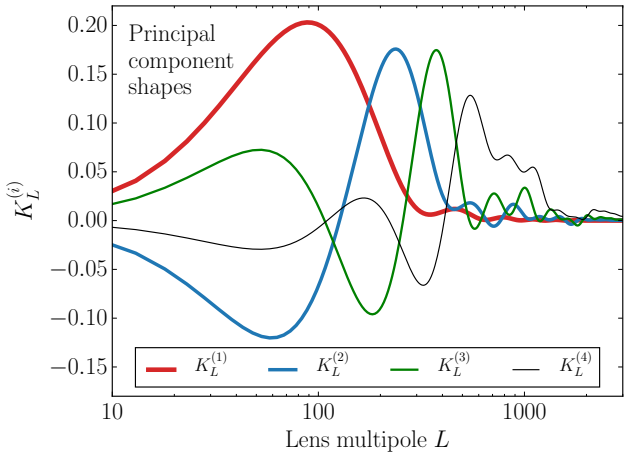

FIG. 1. Functions $K_L^{(i)}$ corresponding to the four principal components of the lens potential best measured by the Planck lensed TT power spectrum, determined from the `liteTT` likelihood.

III. MODEL-INDEPENDENT LENSING CONSTRAINTS

Measuring the lens principal components from the Planck temperature, polarization and lensing reconstruction power spectra provides a new means of extracting and comparing the various sources of lens information in the CMB. This comparison presents a direct and model-independent consistency test of the lensing information [24] and in the ΛCDM model context enables an internal consistency check of the ΛCDM parameters inferred from CMB power spectra information from recombination and from lens information. This is particularly relevant given the known preference for excess lensing in the Planck temperature data [19, 22].

We start by characterizing the information in the lensing reconstruction data, which also determines the number of lens principal components required for our comparative analysis. We then discuss constraints on $\Theta^{(i)}$ from the temperature and polarization power spectra and focus on the two leading principal components. We also derive $\Theta^{(i)}$ from the recombination or unlensed information in the power spectrum in the ΛCDM model as a check of its internal consistency. We finish by commenting on robustness of our results with respect to various analysis choices.

A. Reconstruction constraints

The principal component decomposition of the lens power spectrum described in §II B is optimized for the temperature power spectrum analysis but can also be used to analyze the reconstruction data. Even though we will be mainly interested in the first two components for comparisons with the other analyses, it is important to retain a sufficient number of higher components so that their marginalization does not affect the lower ones.

In practice we choose the number of principal components according to whether the data can constrain them better than a weak theoretical prior. We choose flat tophat priors on $\Theta^{(i)}$ within a range where the variation in $C_L^{\phi\phi}$ is within a factor of 1.5 of $C^{\phi\phi}_{L,\rm fid}$. These weak priors are meant to eliminate cases that would be in conflict with other measurements of large scale structure or imply unphysically large amplitude high frequency features in $C_L^{\phi\phi}$.

In Fig. 2 we show constraints from the lensing reconstruction likelihood `PP` on the first four $\Theta^{(i)}$ for the cases where we allow four or five lens PCs to vary. For $\Theta^{(3)}$ and $\Theta^{(4)}$ the edges of the box represent the prior and so the 4th component is nearly prior limited. Correspondingly, the addition of $\Theta^{(5)}$ does not significantly affect constraints on $\Theta^{(1)}$ and $\Theta^{(2)}$ which will be important for evaluation of the tensions in the data. We therefore standardize on four lens PCs unless otherwise specified, with higher lens PCs set to zero, which is their fiducial value.

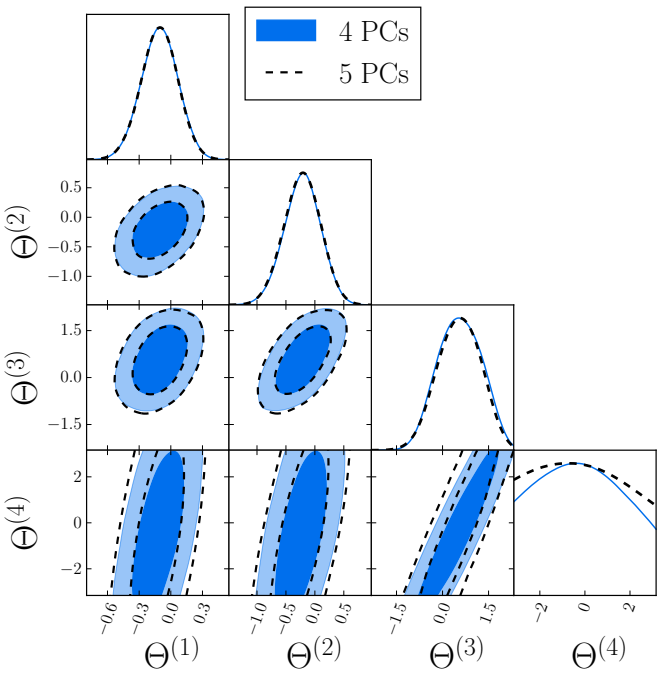

FIG. 2. Lens reconstruction constraints from PP on lens PCs (68% and 95% CL). The analysis with the fiducial four PCs (blue solid) and with an additional fifth PC marginalized (dashed) give nearly identical results for the first two PCs. Higher PCs are fixed to zero, their fiducial value.

Another way to visualize why 4 PCs suffices is to construct the lens power spectrum out of them as

$$C^{\phi\phi}_{L,\rm filt} = C^{\phi\phi}_{L,\rm fid} \exp\left(\sum_{i=1}^{4} K_L^{(i)}\,\Theta^{(i)}\right). \qquad (2)$$

and compare it to the lens reconstruction data itself. In Fig. 3, we show this comparison. The 4 PC construction represents smooth deviations that are allowed by the data. Fluctuations that are not represented by the functional form of the PCs shown in Fig. 1 are not captured by the construction, for example the fluctuation in the data around $L = 330$. Thus the PC construction does not represent direct, but rather filtered, constraints on $C_L^{\phi\phi}$. To compare PC constraints from other sources to the lens reconstruction constraints, it is important to compare their implications for $C^{\phi\phi}_{L,\rm filt}$ rather than $C_L^{\phi\phi}$ directly. This PC filter has the benefit of producing smooth functional constraints utilizing the full data set at the expense of highly correlating constraints at different multipoles.

B. Temperature constraints

We analyze the TT+lowTEB likelihood for 4 PCs with the weak theoretical priors discussed in the previous section. To focus on the region consistent with lens reconstruction, we impose an additional data-driven prior. As shown in the previous section, lensing reconstruction constrains $\Theta^{(1)}$ and $\Theta^{(2)}$ significantly better than the theoretical prior from the previous section, we thus consider restricting these two variables further. As we will see, $\Theta^{(1)}$ drives the tension between reconstruction and temperature constraints; for this reason we do not strengthen the prior on it. On the other hand, we restrict $\Theta^{(2)}$ to lie

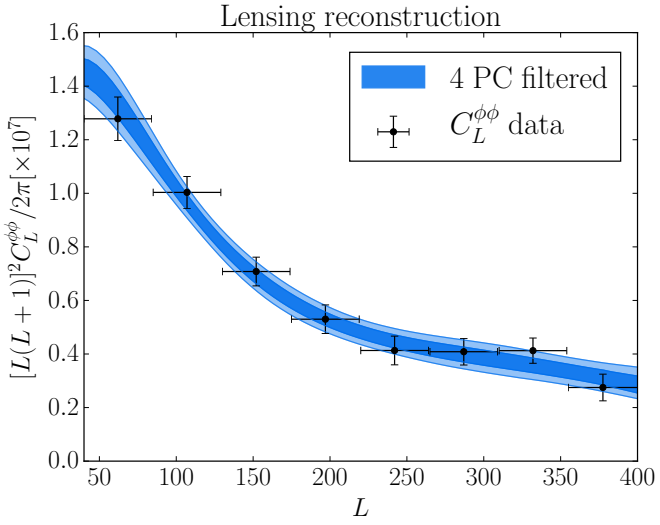

FIG. 3. Lens reconstruction constraints from PP on the lens power spectrum filtered through the 4 PC analysis $C^{\phi\phi}_{L,\rm filt}$ (blue, 68% and 95% CL). The points correspond to the measured Planck values included in the PP likelihood. Although the points are only weakly correlated, PC filtering through Eq. (2) utilizes all data points for each multipole leading to a smoother but correlated constraint.

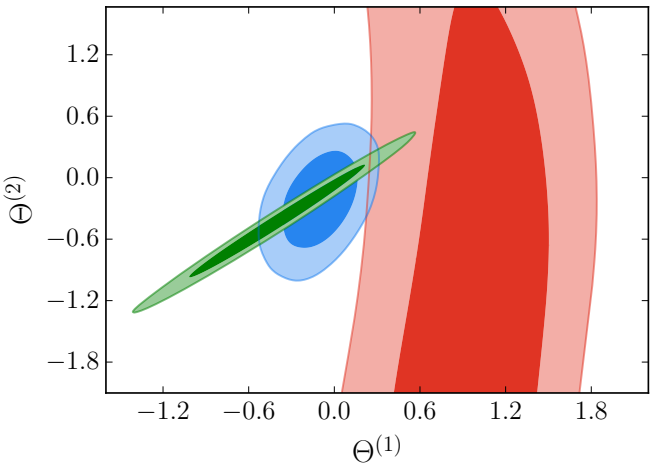

FIG. 4. CMB power spectrum constraints on lens PCs $\Theta^{(1)}$ and $\Theta^{(2)}$ from TT+lowTEB (red, 68% and 95% CL) compared with lens reconstruction PP from Fig. 2 (blue) and ΛCDM predictions based on unlensed parameters $\tilde{\theta}_A$ from TT+lowTEB (green). The fiducial 4 PC analysis is used in all cases.

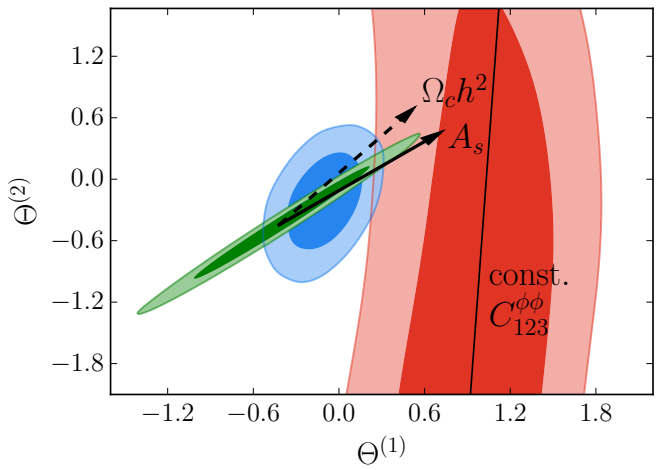

FIG. 5. Physical interpretation of constrained directions from Fig. 4. The line approximates the degeneracy direction of the TT+lowTEB (red) contour and correspond to a line of constant $C_{123}^{\phi\phi}$. Arrows shows changes in $C_L^{\phi\phi}$ caused by increasing A_s (solid) and $\Omega_c h^2$ (dashed) in ΛCDM while keeping the other parameters in Tab. II fixed.

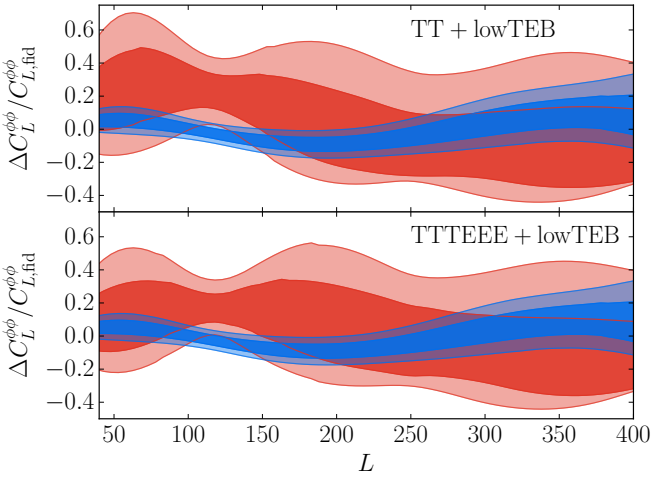

FIG. 6. CMB power spectrum constraints on fractional deviations in the 4 PC filtered lens power spectrum from the fiducial model $\Delta C_L^{\phi\phi}/C_{L,\mathrm{fid}}^{\phi\phi}$ (red, 68% and 95% CL) compared with that of lens reconstruction from Fig. 3 (blue). Top panel shows constraints from TT+lowTEB and bottom panel from TTTEEE+lowTEB which adds high-ℓ polarization. Above $L \sim 175$, CMB power spectrum constraints mainly reflect priors on the 4 PC amplitudes.

within six standard deviations from the mean value from the reconstruction analysis that considers 4 PCs. We retain this prior even for analyses in which $\Theta^{(4)}$ is fixed to its fiducial value. We shall see that the tension between power spectra and lensing reconstruction information on lensing is weaker than 6σ and so this prior does not artificially increase the tension. It therefore just excludes the parameter space that would be grossly ruled out by reconstruction data and is used mostly for visualization purposes.

As expected, TT+lowTEB data constrain mainly one principal component with $\Theta^{(2)}$ limited by the priors and $\Theta^{(3)}$ and $\Theta^{(4)}$ completely dominated by them. In Fig. 4 we show the constraints (red contours) in the $\Theta^{(1)} - \Theta^{(2)}$ plane out to the edge of the $\Theta^{(2)}$ prior. Because the PCs were constructed from a Fisher forecast, the constrained direction is nearly but not perfectly aligned with $\Theta^{(1)}$, leaving a slight correlation between the two parameters. In Fig. 5 we show that the degenerate direction for the TT+lowTEB analysis corresponds approximately to constant $C_{123}^{\phi\phi}$, whereas contours of constant $\Theta^{(1)}$ correspond approximately to $C_{127}^{\phi\phi}$ as determined by the zero crossing of $K_L^{(2)}$ in Fig. 1.

For comparison we in Fig. 4 also show the constraints from lens reconstruction (blue contours). The two constraints are in tension with each other in that the two contours only overlap in their 95% CL regions. Moreover, this tension is model independent: no change in the shape of $C_L^{\phi\phi}$ allowed by the 4 PCs can resolve it.

A complementary view of the tension is presented in Fig. 6 (top panel), where we compare posterior constraints on $C_L^{\phi\phi}$ as filtered through the first 4 PCs via Eq. (2) from PP and from the TT+lowTEB analysis above; for the ease of comparison we show fractional difference from the fiducial model. The constraints from the latter are strongest around $L \sim 125$ and around this area favor more lensing power than preferred by the reconstruction data. Although changes in the shape of $C_L^{\phi\phi}$ can bring agreement between the two away from this regime, tension remains there independent of the model.

Within the ΛCDM we can further study the origin of this tension. From the same TT+lowTEB analysis, we can predict $C_L^{\phi\phi}$ from information in the unlensed CMB power spectra at each sampled parameter point $\tilde{\theta}_A$ under the ΛCDM assumption. We can then translate this prediction into $\Theta^{(i)}$ by inverting Eq. (1). These ΛCDM predictions, shown as the green contours in Fig. 4, can be directly compared with the lensing PC measurements themselves. Some tension between the red and green contours is visible, as they overlap only at the $\sim 95\%$ confidence levels; this is the lensing PC version of the well-known A_L lensing anomaly in the high-ℓ TT data.

Unlike A_L, which only indirectly specifies $C_L^{\phi\phi}$ by changing its amplitude relative to the ΛCDM prediction point by point in its parameter space, PCs directly change the amplitude and shape of $C_L^{\phi\phi}$. This allows us to more directly quantify the origin of lensing tension. It is straightforward to trace back the origin of the ΛCDM degenerate direction in the $\Theta^{(1)} - \Theta^{(2)}$ plane: arrows in Figure 5 show how these two parameters change when we increase values of A_s and $\Omega_c h^2$ (at fixed θ_* and other parameters; constructed from the partial derivatives listed in Tab. III), which within ΛCDM are the two parameters with dominant effects on $C_L^{\phi\phi}$. Given current constraints

TABLE III. Dependence of $C_L^{\phi\phi}$ on selected ΛCDM parameters

	$\Theta^{(1)}$	$\Theta^{(2)}$
$\partial\Theta^{(i)}/\partial(\Omega_c h^2)$	82.0	99.1
$\partial\Theta^{(i)}/\partial \ln A_s$	7.45	5.95

on τ, the degenerate direction is mainly aligned with that of A_s, with a smaller contribution from $\Omega_c h^2$. On the other hand, the lensing PC constraints from `TT+lowTEB` mainly reflect $\Theta^{(1)}$ and are driven by the $L \sim 125$ region of the lens power spectrum that is best measured by the TT spectrum. Though they are lens model independent, the lens reconstruction constraints are in good agreement with the ΛCDM constraints in green. Furthermore, the near alignment of the directions of the ΛCDM constraints and the reconstruction constraints (blue) also suggest that the tension with power spectrum constraints (red) cannot be significantly relieved by going beyond ΛCDM.

We can also compare the temperature power spectrum of the maximum likelihood ΛCDM model with that of the maximum likelihood model with lens PCs to see what part of the temperature power spectrum data drives this preference for anomalous lensing; we show cases where either one or four lens PCs are varying from their fiducial values. In Fig. 7, we show the residuals relative to the best fit ΛCDM model scaled by the cosmic variance errors

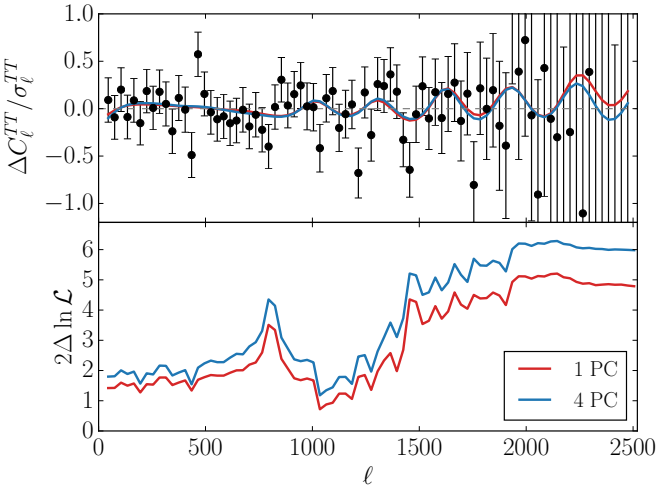

FIG. 7. Top: Residuals between Planck temperature power spectrum measurements and the best fit ΛCDM model given the `TT+lowTEB` likelihood (points, scaled to cosmic variance errors per multipole σ_ℓ^{TT}). The blue (red) line shows the best fit once we allow four (one) lensing PCs to vary, with fixed foregrounds. Bottom: improvement in the cumulative $2\ln\mathcal{L}(\leq \ell)$ over ΛCDM for the same models showing that most of the improvement is from the first PC and corresponds to smoother acoustic peaks in the $\ell \sim 1250 - 1500$ range.

per multipole,

$$\sigma_\ell^{TT} = \sqrt{\frac{2}{2\ell+1}} C_\ell^{TT}, \tag{3}$$

evaluated at the fiducial ΛCDM model. Notice the Planck data are binned and so the standard deviations of the data can be smaller than σ_ℓ^{TT}. When searching for the best fit PC model, we fix the foreground parameters to their best fit ΛCDM values from the `TT+lowTEB` likelihood, for which the visualization of the Planck data points were derived. In the lower panel of Fig. 7, we then show the cumulative improvement over ΛCDM in $2\Delta\ln\mathcal{L}$ of the fit as a function of the maximum ℓ.[*3] The total reaches $2\Delta\ln\mathcal{L} = 6.0$ at the highest multipole employed in the analysis when allowing four lens PCs to vary. As is visible from the figure, $2\Delta\ln\mathcal{L} \approx 5$ of 6 comes from the first lens PC, in agreement with our previous statement that majority of the lensing information in the temperature power spectra is well captured by a single lensing component.

The data points show oscillatory residuals with respect to the ΛCDM model in the ℓ range 1250–1500 that indicate smoother acoustic oscillations (see also [20, 30]). Correspondingly, the largest part of the improvement arises through fitting these residuals by increasing the smoothing due to lensing, though notable contributions come from the `lowTEB` part of the likelihood. The latter is associated with the ability to lower TT power at $\ell \lesssim 30$.

These improvements allowed by releasing $C_L^{\phi\phi}$ from its ΛCDM value also lead to shifts in cosmological parameters; these shifts are summarized in Figure 8, for the case where the foreground parameters are again allowed to vary. In ΛCDM, preference for fitting the oscillatory residuals pushes values of $\Omega_c h^2$ and A_s up, which then forces other ΛCDM parameters to compensate. In the PC case, lensing parameters $\Theta^{(i)}$ play this role and allow $\Omega_c h^2, A_s$ to drop. This drop and the associated changes in other parameters allows for a lower low-ℓ TT power with respect to the acoustic peaks and therefore also allows a better fit to the anomalously low TT power at $\ell \lesssim 30$. In models with the ΛCDM expansion history such a drop also simultaneously raises H_0 to (69.1 ± 1.2) km/s/Mpc and can help relieve tension with the local distance ladder measurements [31].

Taken at face value, these mild tensions and their alleviation with lensing PC parameters would motivate explorations of additional physics at low z which modify the lens potential. However, independent of the model for the lens potential, tension with lensing reconstruction remains.

[*3] Due to different binning schemes used by the Planck collaboration for their best fit TT power spectrum and binned TT likelihood, we use the *unbinned* Planck TT likelihood to obtain this plot.

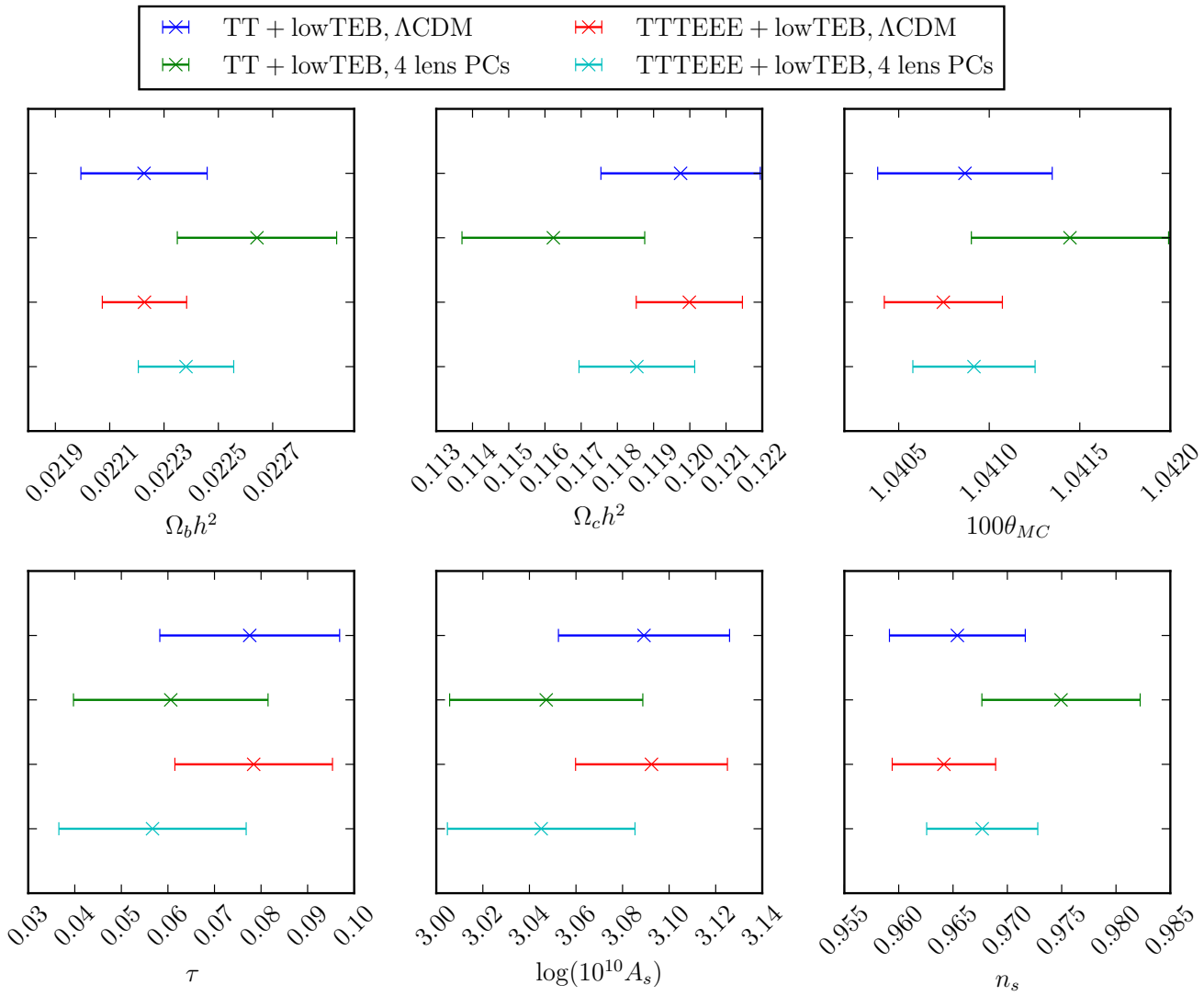

FIG. 8. Cosmological parameters constraints from `TT+lowTEB` and `TTTEEE+lowTEB` with the fiducial lensing 4 PC analysis (green, cyan) compared with ΛCDM (blue, red). The former correspond to constraints on $\tilde{\theta}_A$ from the unlensed power spectra.

C. Polarization constraints

Next, we add the high-ℓ polarization constraints using the `TTTEEE+lowTEB` likelihood; the various constraints on $\Theta^{(1,2)}$ are shown in Fig. 9. The 2015 Planck polarization data is known to be subject to systematics that make lensing conclusions unstable [19] and thus we consider their addition separately.

The main change is a shift in the contours to lower values of $\Theta^{(1)}$ but with tighter errors. This shift is driven by the C_ℓ^{TE} data; lensing constraints from C_ℓ^{EE} are notably weaker and additionally favor even more lensing than C_ℓ^{TT} does [19]. With polarization, the tension between CMB power spectra and lens reconstruction constraints only mildly relaxes. This is because of the combination of the shift and the smaller errors in Fig. 9. In Fig. 6 (bottom), we also show the impact of adding polarization data on the filtered $C_L^{\phi\phi}$ constraints. Correspondingly, polarization data only mildly decreases the significance of tension around $L \sim 125$.

The internal tension between temperature-polarization power spectra and the ΛCDM prediction in green relaxes somewhat more. This is because polarization favors the high $\Omega_c h^2$ values of the best fit ΛCDM model to `TT+lowTEB` (as shown in Fig. 8) due to unusually strong TE constraints in the region around $\ell \sim 200$ [30]. This preference is in a region that is relatively unaffected by lensing and so remains after releasing $C_L^{\phi\phi}$. Raising $\Omega_c h^2$ in ΛCDM has the effect of increasing lensing making the temperature-polarization power spectra and ΛCDM somewhat more consistent.

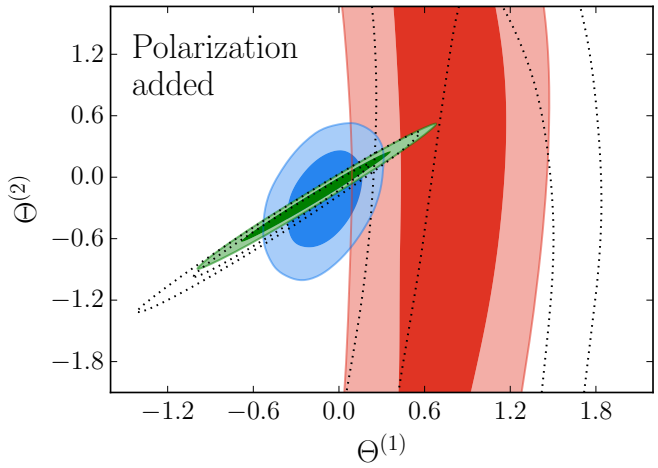

FIG. 9. Impact of high-ℓ polarization on PC constraints from Fig. 4 (repeated with dotted contours for comparison). While tension between the `TTTEEE+lowTEB` (red) and the ΛCDM results (green) weakens slightly, its tension with `PP` remains nearly the same due to its shift and reduced errors in the $\Theta^{(1)}$ direction.

D. Robustness tests

To check that the results are stable with respect to the considered number of lens PCs, we repeat our analysis with $\Theta^{(4)}$ fixed to its fiducial value. In Fig. 10 (top) we show that this does not significantly alter the various constraints on $\Theta^{(1)}, \Theta^{(2)}$ based on `TT+lowTEB` and `PP`. The same conclusion holds when polarization data are added.

We also repeat our analysis with a stronger theoretical prior (with four lens PCs varying) – for $\Theta^{(3)}$ and $\Theta^{(4)}$ we restrict the variation in $C_L^{\phi\phi}$ to be within a factor of 1.4 of $C_{L,\rm fid}^{\phi\phi}$, instead of our default 1.5, while we demand $\Theta^{(2)}$ to be within five standard deviations from the mean value determined from the `PP` likelihood. In Fig. 10 (bottom) we show that impact of the theoretical prior on the tension is negligible.

In our analysis we have so far fixed the unlensed CMB to the power spectra allowed by ΛCDM. Given the lensing model-independence of the tension, it is also interesting to ask whether additional physics at recombination can relax it. We can never completely eliminate this possibility for resolution of tension with our methodology, as effects of this new physics might mimic lensing in the CMB power spectrum while not affecting the higher point moments important in lens reconstruction. On the other hand, we can show that the additional physics cannot be simply a change in the effective number of light relativistic species $N_{\rm eff}$. When adding this parameter to the unlensed parameters $\tilde{\theta}_A$ and marginalizing over it, we find that the tension between high-ℓ TT and lensing reconstruction constraints and the internal lensing tension are both still present and similarly significant.

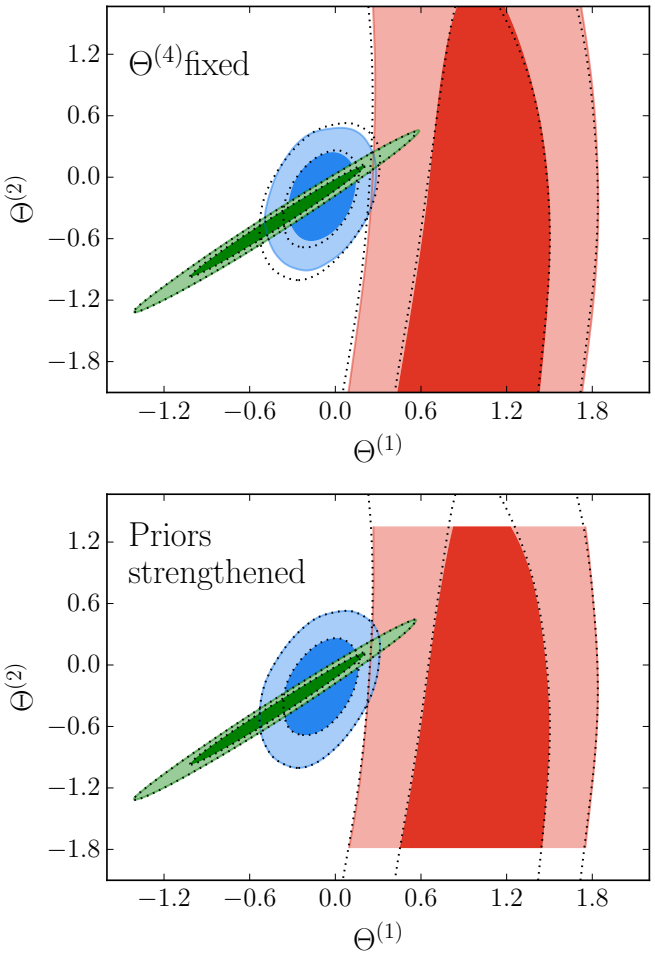

FIG. 10. Robustness checks on PC constraints from Fig. 4 (repeated with dotted contours for comparison). Top: $\Theta^{(4)}$ fixed to its fiducial value instead of marginalized over. Bottom: stronger theoretical prior on $\Theta^{(i)}$ (see the text). Neither change significantly impacts tension between the lensing measurements.

IV. SIGNIFICANCE OF THE TENSIONS

Having illustrated the existence of lensing tensions in the Planck CMB data, we now turn to quantifying their significance. We start by defining a robust single statistic to compare between the various sources of lensing information. We then discuss the significance of the model-independent tension between lensing constraints from Planck temperature/polarization power spectra and lens reconstruction. After that we focus on a special case of ΛCDM with a freely floating amplitude of the lensing potential, which allows us to compare with previous literature and address the significance of the internal tensions between ΛCDM lensing constraints from within the CMB power spectra alone.

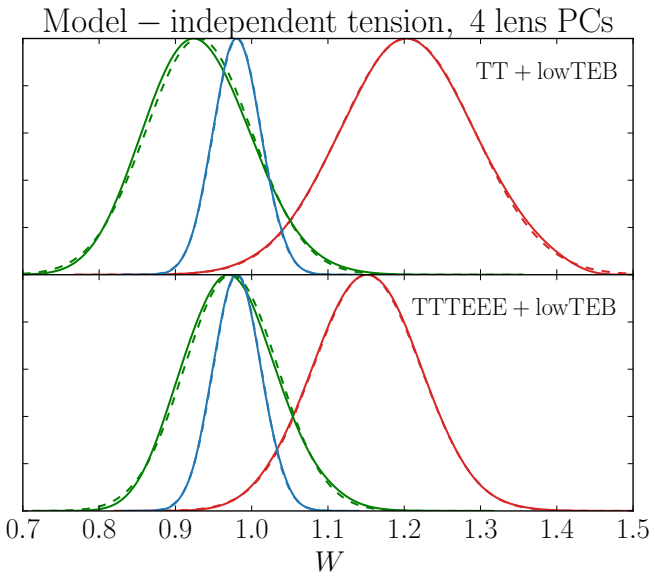

FIG. 11. Posterior probability distribution for the lensing tension parameter W as determined from the fiducial 4 PC analysis of lens reconstruction PP (blue), and CMB power spectra TT+lowTEB (red, top) and TTTEEE+lowTEB (red, bottom). In green we show constraints on W derived from $\tilde{\theta}_A$, obtained under the assumption of ΛCDM from either TT+lowTEB or TTTEEE+lowTEB. Dashed lines show Gaussian distributions with the same means and variances.

TABLE IV. Tension significances when comparing W constraints from a reference data set to CMB power spectra constraints

ref. data	$C_L^{\phi\phi}$ freedom	TT+lowTEB	TTTEEE+lowTEB
PP	4 PCs	2.4	2.2
PP	amplitude $\mathcal{A}$	2.4	2.4
$\tilde{\theta}$ unlensed	amplitude $\mathcal{A}$	2.4	2.1

A. Tension statistics

In order to quantify the tension simply and cleanly, we seek to find a single auxiliary parameter whose distribution reflects the best constraints and is as close as possible to Gaussian in each of the lensing measurements. For two such measurements, a natural tension statistic to use is the shift in the means $|\mu_1 - \mu_2|$. To the extent that the parameter posteriors are Gaussian distributed, the shift itself is predicted to be Gaussian distributed with a variance that is the sum of the two variances, $\sigma^2 = \sigma_1^2 + \sigma_2^2$. Therefore, the significance of the measured shift in units of σ is given by

$$T = \frac{|\mu_1 - \mu_2|}{\sqrt{\sigma_1^2 + \sigma_2^2}}. \tag{4}$$

To choose the parameter itself, note that the main source of tension is the first principal component $\Theta^{(1)}$ (see Fig. 4). However, to have the posterior distributions well approximated by Gaussian distributions, we instead choose

$$W \equiv \exp\left(K_{123}^{(1)}\Theta^{(1)}\right). \tag{5}$$

W is independent of the higher lens PCs, as these are not constrained by the temperature and polarization power spectra and thus do not add to the tension.

The scaling factor $K_{123}^{(1)}$ makes W the ratio of the 1 PC filtered and fiducial $C_L^{\phi\phi}$ evaluated at $L = 123$ (see Eq. (2)). As we will see, the main benefit of W, or in general a smoothly filtered version of $C_L^{\phi\phi}$, is that it represents a weighted average in L of the data even though it appears to be evaluated at a fixed L. As such it employs the constraining power of the full range of the data. This leads to a powerful and robust tension statistic.

This should be contrasted with $C_{123}^{\phi\phi}$ itself or more generally the power spectrum at any single multipole L. Its value depends sensitively on the higher PCs, which increasingly fit noise fluctuations, and so represent an ineffective tension statistic when they are included. With our standard 4 PC analysis, this is not a significant problem for $C_{123}^{\phi\phi}$ itself as we shall see in the next section, but by defining tension in W we make it robust to higher PCs as well and immune to reoptimizing the effective multipole for each case.

B. Model-independent tension

In Fig. 11, we compare posterior distributions for W determined from CMB power spectra through the TT+lowTEB, TTTEEE+lowTEB likelihoods to that determined from reconstruction through the PP likelihood; the two types of distributions overlap only in the tails. Gaussians with the same means and variances describe even these overlap regions accurately, which justifies the use of the tension statistic T. The tension between TT+lowTEB and PP determinations of W is significant at 2.4σ; adding polarization data decreases the tension to 2.2σ. We summarize significance of various tensions in Table IV.

We now consider several robustness checks on this tension. Using the foreground-marginalized high-ℓ TT likelihood liteTT instead of TT in the analysis leads to the same tension significance of 2.4σ. When the data-driven prior on $\Theta^{(2)}$ of six standard deviations from the PP constraint is dropped, the tensions relax both by about 0.1σ. This is caused by the small curvature of the posterior in the $\Theta^{(1)} - \Theta^{(2)}$ plane, visible for example in the red contour in Fig. 9, which leads to an increased overlap with the lensing reconstruction constraints after the projection onto W.

Next we consider robustness to the constraint on the reionization optical depth τ. The upcoming final release of Planck data is expected to improve and potentially change these constraints. Furthermore, constraints on τ depend on the form assumed for the ionization history that is taken to be step-like in the standard analysis

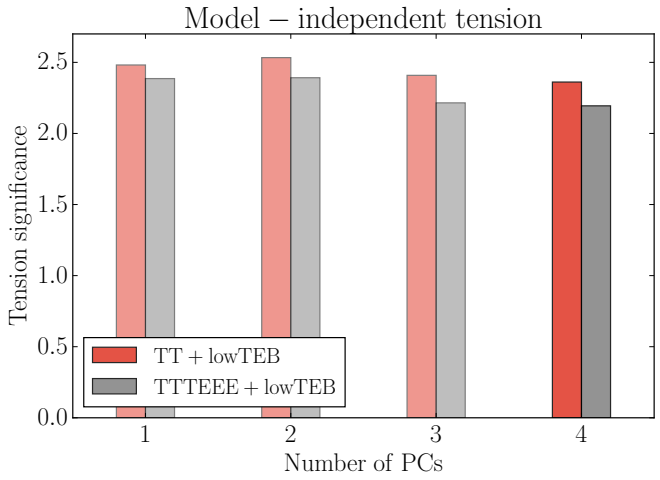

FIG. 12. Significance of the model-independent tension between PP and TT+lowTEB (red) or TTTEEE+lowTEB (gray) determinations of W, as a function of the number of the lensing PCs which are allowed to vary. The tension significance is measured in units of σ, the expected root mean square of the distance between the means. Our default result that uses the 4 PCs is highlighted.

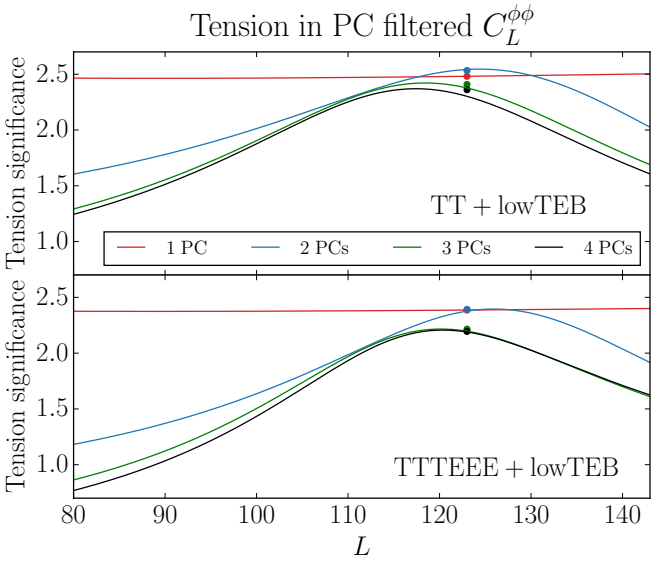

FIG. 13. Tension significance for the PC filtered $C_L^{\phi\phi}$ from PP and TT+lowTEB (top) or TTTEEE+lowTEB (bottom) for various values of L and number of lensing PCs which are allowed to vary. The points represent significance of the model-independent tensions based on W; notice that for one lens PC the two tension statistics are identical at $L = 123$ by construction but that $C_L^{\phi\phi}$ at other values can substantially underestimate tension.

[32, 33]. By isolating the information on the lens power spectrum itself, our tension statistic should be immune to such changes. To quantify the impact of possible future changes in the likelihood, we reevaluate the tension statistic where instead of using TT+lowTEB we constrain W using TT+lowT, together with a τ prior of width 0.02, centered on either 0.04, 0.06 or 0.08. In all three cases the tension changes by less than 0.02σ from the original result obtained using TT+lowTEB. Our conclusions are thus robust to the low-ℓ polarization data and likelihoods. Contrast this with the scaled ΛCDM approach where τ changes the lens power spectrum against which A_L is measured from the temperature power spectrum and lens reconstruction data respectively, leading to sensitivity of A_L constraints to reionization assumptions.

The significance of the tension between TT+lowTEB (or TTTEEE+lowTEB) and PP determinations of W does not notably change when we decrease the freedom in varying $C_L^{\phi\phi}$ by retaining a smaller number of lens PCs in the analysis (see Fig. 12).

Finally, it is possible to demonstrate why W is more robust than $C_L^{\phi\phi}$ at some L that has not been specifically optimized for the model-independent lensing test. First, we can take the full 4 PC filtered construction of $C_L^{\phi\phi}$ depicted in Fig. 6. We show the resulting tension as a function of L in Fig. 13 (black curves) between PP and TT+lowTEB (or TTTEEE+lowTEB). The tension T in $C_L^{\phi\phi}$ constraints at $L \sim 120$ is similar to that in W. On the other hand, choosing other values of L could substantially degrade the ability to identify tension in these cases where the shape of $C_L^{\phi\phi}$ is allowed to vary.

Likewise, an alternate choice of L can make the tension statistic more dependent on the number of lens PCs allowed to vary. In Fig. 13, we also show the results of analyses with 1,2 or 3 lens PCs allowed to vary, where $C_L^{\phi\phi}$ is filtered with the same number of PCs. Again, away from $L \sim 120$ the tension significance can vary widely.

C. ΛCDM and amplitude changes

Besides the weak theoretical prior, the tension quoted in the previous section was derived without any constraints on the shape of the gravitational lensing potential. By allowing the largest possible freedom, it represents a lower limit on the tension present in the data; particular models can restrict this freedom and consequently lead to a larger significance of the tension. As a simple example and to connect with the earlier literature, we investigate here ΛCDM model with a freely floating amplitude of $C_L^{\phi\phi}$.

We therefore model the lensing potential as

$$C_L^{\phi\phi} = \mathcal{A} C_{L,\rm fid}^{\phi\phi}, \tag{6}$$

below we refer to this model as "fid + $\mathcal{A}$" but recall that the fiducial model is set by the best fit ΛCDM parameters in Tab. II. Note that this is different from the standard

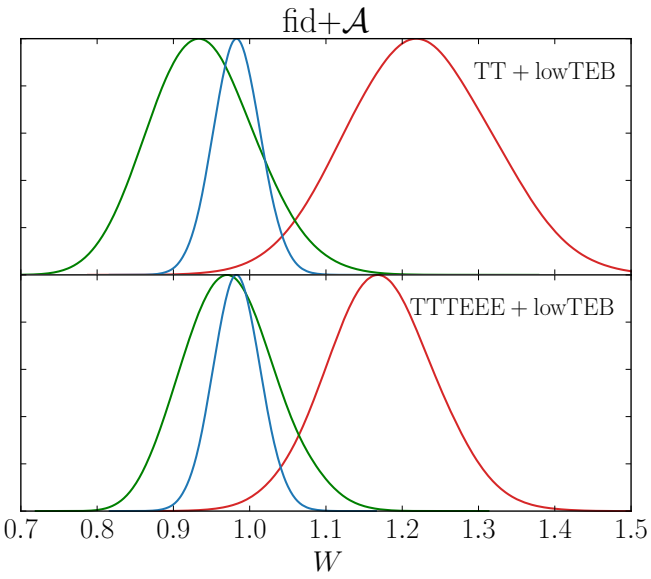

FIG. 14. Posterior probability distributions for the lensing tension parameter W as in Fig. 11 but allowing only for amplitude changes with the fid+$\mathcal{A}$ model.

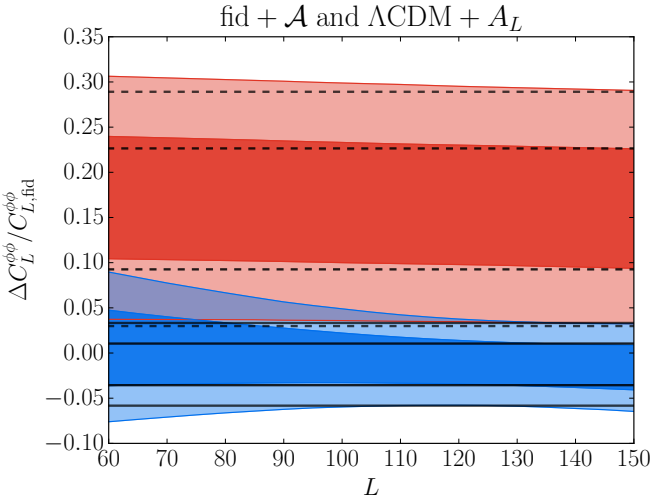

FIG. 15. Constraints on $\Delta C_L^{\phi\phi}/C_{L,\mathrm{fid}}^{\phi\phi}$ as in Fig. 6, but for amplitude and ΛCDM shape variations. The black lines show results from `TT+lowTEB` (dashed) or `PP` (solid) within the fid+$\mathcal{A}$ for amplitude variations. Filled contours are determined from `TT+lowT` within ΛCDM+A_L with a τ prior (red) and separately from `PP` with ΛCDM freedom on the amplitude and shape but with fixed τ, θ_* and a prior on $\Omega_b h^2$ and n_s (blue). Constraints, especially at low L from the latter, depend on which ΛCDM parameters are allowed to separately vary.

A_L and $A_{\phi\phi}$[*4] parameters in that the amplitude multiplies a fixed fiducial model. Constraints on W from these two data sets are shown in Fig. 14 (top). Comparing these two constraints leads to a tension of 2.4σ, the same as the model-independent tension derived in the previous section. When adding polarization data, the tension evaluates to the same 2.4σ, slightly more than the model-independent value; see Fig. 14 for changes in the posteriors. Comparing instead constraints on $\mathcal{A}$ directly leads to the same tension significance both with and without polarization. The good agreement with constraints on $\mathcal{A}$ gives further evidence that W is a powerful and robust tension indicator, even though it is constructed from a single PC.

With W we can also compare the predictions from the unlensed parameters $\tilde{\theta}_A$ in the same fid+$\mathcal{A}$ context. These correspond to the green curves in Fig. 14 and when compared with their red counterparts evaluate to internal tensions significant at 2.4σ for `TT+lowTEB`, respectively 2.1σ for `TTTEEE+lowTEB`.

Within the fid+$\mathcal{A}$ model considered here, constraints on any $C_L^{\phi\phi}$ show the same significance of the tension as $\mathcal{A}$ (see Fig. 15, solid vs. dashed lines). Nonetheless, there are subtleties in using $C_L^{\phi\phi}$ itself as a tension indicator beyond $\mathcal{A}$, even for parameterizations that are motivated by ΛCDM. As we argued above, to quote tension in $C_L^{\phi\phi}$ measurements, one has to exactly specify how much freedom in the lensing potential is allowed; in the PC case, this turns into a sensitivity to the number of PCs involved.

For variations motivated by ΛCDM, one has to carefully specify which parameters are allowed to independently vary between the reconstruction and CMB power spectra analyses. For example, let us take the case of comparing the temperature power spectrum `TT+lowT` and lens reconstruction measurements as commonly considered in the literature. For the former case we further take the usual ΛCDM+A_L approach which allows some variation in the shape of the lensing power spectrum through the cosmological parameters. Without the low-ℓ polarization data, we must specify the prior on τ since it controls A_s through the measured amplitude of the temperature peaks. For definiteness let us take a Gaussian prior of $\tau = 0.07 \pm 0.02$.

Given reconstruction data alone, ΛCDM allows both amplitude and larger shape changes since the cosmological parameters are not constrained by CMB power spectra. For definiteness, let us take the joint posterior of the ΛCDM parameters $\ln A_s, n_s, \Omega_c h^2, \Omega_b h^2$ with Gaussian priors $\Omega_b h^2 = 0.0223 \pm 0.0009$ and $n_s = 0.96 \pm 0.02$. Constraints on $C_L^{\phi\phi}$ when allowing these variations are shown in Fig. 15 (red vs. blue contours). Note that as L decreases, these additional shape variations in $C_L^{\phi\phi}$ weaken the apparent tension.

When one compares constraints on $C_{100}^{\phi\phi}$, this is the

[*4] $A_{\phi\phi}$ is a parameter that scales the lensing potential used in the `PP` but not the one used in the `TT` likelihood.

technique used in Ref. [20][*5]. At $L = 100$ the shape variation only has a mild effect that is further reduced by the shift in both contours so for $C_{100}^{\phi\phi}$ we retain a tension significance of 2.4σ.[*6]

At lower L the shape variations become more important. On the lensing reconstruction side, the ΛCDM parameters are not well constrained and allow values that are inconsistent with the unlensed CMB; this leads to the shape variations noticeable at low L in Fig. 15. Had we allowed even larger freedom in $C_L^{\phi\phi}$ by changing say the prior on n_s on the reconstruction side, the apparent tension would further degrade. On the `TT+lowT` side the ΛCDM parameters are very well constrained, leaving less of an effect on the shape of $C_L^{\phi\phi}$ and the contours mostly reflect uncertainty in the amplitude through A_L. However, when more freedom is granted to the lensing potential, the apparently strong constraints at low L degrade (see Fig. 6), also decreasing the tension. It is thus important to carefully specify the model freedom in using $C_L^{\phi\phi}$ as a statistic. This problem is largely removed by using W which has the same meaning in all models.

V. DISCUSSION

In this work we separate the lensing information from CMB power spectra from the cosmological parameters that control the high redshift physics and thereby illuminate the so-called "lensing tensions" in the Planck CMB data. By modeling the principal components of the lens potential $C_L^{\phi\phi}$ given the Planck CMB power spectra, we isolate the one aspect that is constrained by the data in a model independent way. We then compare this constraint to results from lens reconstruction through the 4 principal components that it constraints to test whether variations in $C_L^{\phi\phi}$ beyond ΛCDM can relax tension between the two different sources of lensing information.

We show that the tension remains between the temperature and lensing reconstruction determinations of $C_L^{\phi\phi}$ even beyond ΛCDM. Previous studies of the Planck lensing anomaly [19–22] considered only the addition of changes in the amplitude of the gravitational lensing potential from ΛCDM predictions. Our technique extends these studies and clarifies the nature of the tension by extracting direct constraints on $C_L^{\phi\phi}$, which obviates the need for directly specifying ΛCDM parameters in interpreting tension, and allowing shape variations from ΛCDM.

Even allowing for shape and amplitude variations beyond ΛCDM, the tension between temperature and lensing reconstruction remains at a level of 2.4σ, essentially the same as with amplitude variations alone. The significance decreases mildly to 2.2σ when polarization data are taken into account unlike in the case of amplitude variations; this drop is driven by preference of the TE data for less lensing.

We evaluate these tension significances by using a simple difference of the means statistic tension on a simple function of the first principal component. For the Planck 2015 data which measure only a single aspect of lensing from CMB power spectra, this provides a simple but powerful, robust, and lensing model independent quantification of tension. Our technique can be easily applied to future CMB data sets, where more and mutually correlated aspects are measured [24, 25], with a suitable generalization of tension statistics (e.g. [34]).

This tension is driven by the multipole range $\ell \sim 1250 - 1500$ in the TT data which prefers smoother acoustic peaks than predicted by the standard physics at recombination and lensing reconstruction. While new physics at recombination could in principle relieve tension, it cannot be relieved by adjusting the relativistic degrees of freedom through $N_{\rm eff}$.

By separating information in the lensed CMB power spectra into lensing and unlensed components, we also enable a consistency check on the ΛCDM cosmological model. Because the ΛCDM prediction based on constraints to the unlensed CMB is consistent with the lensing reconstruction constraints, the internal consistency check fails at similar significance as the comparison of the temperature – lensing reconstruction determinations of lensing potential. Addition of polarization data again decreases the significance of the tension, more so this time due to preference for high $\Omega_c h^2$ in the TE data.

While these tensions may point to systematic errors or a statistical fluke that is resolved by more data and improved data reduction, our technique of extracting direct constraints on the lensing potential from CMB power spectra data should continue to provide a robust and powerful tool for testing the consistency of ΛCDM and searching for new physics in the future.

ACKNOWLEDGMENTS

We thank Niayesh Afshordi, Neal Dalal, Marius Millea and Marco Raveri for useful discussions. This work was supported by NASA ATP NNX15AK22G and the Kavli Institute for Cosmological Physics at the University of Chicago through grant NSF PHY-1125897 and an endowment from the Kavli Foundation and its founder Fred Kavli. WH was additionally supported by U.S. Dept. of Energy contract DE-FG02-13ER41958 and the Simons Foundation. We acknowledge use of the CAMB and CosmoMC software packages. This work was completed in part with resources provided by the University of Chicago Research Computing Center. PM thanks the Perimeter Institute for Theoretical Physics where part of this work was performed. Research at Perimeter Institute is sup-

[*5] Marius Millea, private communication

[*6] The small difference from the value 2.3σ quoted in Ref. [20] can be caused by different analysis choices.

ported by the Government of Canada through the Department of Innovation, Science and Economic Development and by the Province of Ontario through the Ministry of Research and Innovation.

[1] A. Lewis and A. Challinor, Phys. Rept. **429**, 1 (2006), arXiv:astro-ph/0601594 [astro-ph].
[2] K. M. Smith, O. Zahn, and O. Dore, Phys. Rev. **D76**, 043510 (2007), arXiv:0705.3980 [astro-ph].
[3] C. M. Hirata, S. Ho, N. Padmanabhan, U. Seljak, and N. A. Bahcall, Phys. Rev. D **78**, 043520 (2008).
[4] D. Hanson *et al.* (SPTpol), Phys. Rev. Lett. **111**, 141301 (2013), arXiv:1307.5830 [astro-ph.CO].
[5] S. Das *et al.*, Phys. Rev. Lett. **107**, 021301 (2011), arXiv:1103.2124 [astro-ph.CO].
[6] R. Keisler *et al.*, Astrophys. J. **743**, 28 (2011), arXiv:1105.3182 [astro-ph.CO].
[7] P. A. R. Ade *et al.* (The Planck Collaboration), Astron. & Astrophys. **571**, A17 (2014), arXiv:1303.5077.
[8] R. Keisler *et al.* (SPT), Astrophys. J. **807**, 151 (2015), arXiv:1503.02315 [astro-ph.CO].
[9] P. A. R. Ade *et al.* (Planck), Astron. Astrophys. **594**, A15 (2016), arXiv:1502.01591 [astro-ph.CO].
[10] P. A. R. Ade *et al.* (BICEP2, Keck Array), (2016), arXiv:1606.01968 [astro-ph.CO].
[11] B. D. Sherwin *et al.*, ArXiv e-prints (2016), arXiv:1611.09753.
[12] U. Seljak, Astrophys. J. **463**, 1 (1996), arXiv:astro-ph/9505109 [astro-ph].
[13] M. Zaldarriaga, Phys. Rev. **D62**, 063510 (2000), arXiv:astro-ph/9910498 [astro-ph].
[14] W. Hu, Phys. Rev. **D64**, 083005 (2001), arXiv:astro-ph/0105117 [astro-ph].
[15] W. Hu and T. Okamoto, Astrophys. J. **574**, 566 (2002), arXiv:astro-ph/0111606 [astro-ph].
[16] T. Okamoto and W. Hu, Phys. Rev. **D67**, 083002 (2003), arXiv:astro-ph/0301031 [astro-ph].
[17] C. M. Hirata and U. Seljak, Phys. Rev. **D68**, 083002 (2003), arXiv:astro-ph/0306354 [astro-ph].
[18] K. M. Smith, D. Hanson, M. LoVerde, C. M. Hirata, and O. Zahn, JCAP **1206**, 014 (2012), arXiv:1010.0048 [astro-ph.CO].
[19] P. A. R. Ade *et al.* (Planck), Astron. Astrophys. **594**, A13 (2016), arXiv:1502.01589 [astro-ph.CO].
[20] N. Aghanim *et al.* (Planck), Astron. Astrophys. **607**, A95 (2017), arXiv:1608.02487 [astro-ph.CO].
[21] G. E. Addison, Y. Huang, D. J. Watts, C. L. Bennett, M. Halpern, G. Hinshaw, and J. L. Weiland, Astrophys. J. **818**, 132 (2016), arXiv:1511.00055 [astro-ph.CO].
[22] P. A. R. Ade *et al.* (Planck), Astron. Astrophys. **571**, A16 (2014), arXiv:1303.5076 [astro-ph.CO].
[23] J. Carron, A. Lewis, and A. Challinor, JCAP **1705**, 035 (2017), arXiv:1701.01712 [astro-ph.CO].
[24] P. Motloch, W. Hu, and A. Benoit-Lévy, Phys. Rev. **D95**, 043518 (2017), arXiv:1612.05637 [astro-ph.CO].
[25] P. Motloch and W. Hu, (2017), arXiv:1709.03599 [astro-ph.CO].
[26] A. Lewis and S. Bridle, Phys. Rev. **D66**, 103511 (2002), arXiv:astro-ph/0205436 [astro-ph].
[27] A. Gelman and D. B. Rubin, Statist. Sci. **7**, 457 (1992).
[28] K. M. Smith, W. Hu, and M. Kaplinghat, Phys. Rev. **D74**, 123002 (2006), arXiv:astro-ph/0607315 [astro-ph].
[29] R. Adam *et al.* (Planck), Astron. Astrophys. **596**, A108 (2016), arXiv:1605.03507 [astro-ph.CO].
[30] G. Obied, C. Dvorkin, C. Heinrich, W. Hu, and V. Miranda, Phys. Rev. **D96**, 083526 (2017), arXiv:1706.09412 [astro-ph.CO].
[31] A. G. Riess, S. Casertano, W. Yuan, L. Macri, J. Anderson, J. W. MacKenty, J. B. Bowers, K. I. Clubb, A. V. Filippenko, D. O. Jones, and B. E. Tucker, Astrophys. J. **855**, 136 (2018), arXiv:1801.01120 [astro-ph.SR].
[32] W. Hu and G. P. Holder, Phys. Rev. **D68**, 023001 (2003), arXiv:astro-ph/0303400 [astro-ph].
[33] C. H. Heinrich, V. Miranda, and W. Hu, (2016), arXiv:1609.04788 [astro-ph.CO].
[34] S. Kullback and R. A. Leibler, Ann. Math. Statist. **22**, 79 (1951).